Available online at www.sciencedirect.com
SCIENCE DIRECT®
International Journal of Heat and Mass Transfer 48 (2005) 4090–4102
International Journal of HEAT and MASS TRANSFER
www.elsevier.com/locate/ijhmt

An analytical study of heat transfer in a finite tissue region with two blood vessels and general Dirichlet boundary conditions

Devashish Shrivastava, Robert Roemer *

Department of Mechanical Engineering, University of Utah, Salt Lake City, UT 84112, USA

Received 27 July 2004; received in revised form 9 March 2005
Available online 20 June 2005

Abstract

Vessel–vessel and vessel–tissue heat transfer rates are defined and explicitly quantified, for the first time, for a uniformly heated, finite, circular tissue region with two arbitrarily imbedded circular vessels and general Dirichlet boundary conditions. These heat transfer rates are obtained using an exact analytical solution for the tissue temperature field that is derived herein. Based on these heat transfer rates two different types of Poisson conduction shape factors (PCSFs) are defined. One is related to the vessel–vessel heat transfer rate (VVPCSF) and the other is related to the vessel–tissue heat transfer rates (VTPCSF). Two, conventional, alternative formulations for the VTPCSFs are studied; one is based on the difference between the average vessel wall and tissue boundary temperatures, and the other on the difference between the average vessel wall and the average tissue matrix temperatures. The effects of the angularly varying, non-uniform boundary conditions, the source term and the diameters and locations of the two vessels on these heat transfer rates and PCSFs are studied for the typical case of vessels cooling a tissue; i.e., when the average vessel wall boundary temperatures are lower than the average tissue boundary temperature. Results show that first, the effects of vessel wall temperature fluctuations on both the vessel–vessel and the vessel–tissue heat transfer rates are significant. Second, unlike the vessel wall temperature fluctuations, fluctuations at the outer tissue boundary affect only the vessel–tissue heat transfer rates. They do not affect the vessel–vessel heat transfer rates. Third, when strong fluctuations are present on the vessel walls and outer tissue boundary the shape factors are dependent on the shape of the fluctuations, and are thus very problem specific. Further, the analytical solution procedure used to derive the solution for the temperature field and the methodology developed to quantify the heat transfer rates are general and can be extended for the case of 'N' arbitrarily located vessels.

1. Introduction

Due to the postulated importance of counter-current blood circulation in determining the tissue temperature distribution [1–7], the effect of the counter-current blood circulation on the tissue temperature distributions has been extensively studied for bio-heat transfer

* Corresponding author. Tel.: +1 801 585 5631; fax: +1 801 585 9826.
E-mail address: bob.roemer@utah.edu (R. Roemer).

0017-9310/$ - see front matter © 2005 Elsevier Ltd. All rights reserved.
doi:10.1016/j.ijheatmasstransfer.2005.04.005

Nomenclature

A_t area of the tissue, $\pi(r_{tw}^2 - r_{vw1}^2 - r_{vw2}^2)$
a_{vi} distance between the centers of the tissue and the ith vessel, $i = 1,2$ (m)
f_{vwi} temperature at vessel wall $i = 1,2$ (K)
f_{tw} temperature at the tissue boundary (K)
g''' uniform source term in the tissue per unit volume (W/m^3)
k conductivity of the tissue (W/(m K))
$q_{vw1-vw2}$ heat transfer from vessel wall one to vessel wall two (W/m)
q_{tw-vw1} heat transfer from tissue to vessel wall one (W/m)
q_{tw-vw2} heat transfer from tissue to vessel wall two (W/m)
$q_{total,vw1}$ total heat transfer to vessel wall one (W/m)
$q_{total,vw2}$ total heat transfer to vessel wall two (W/m)
r radial distance (m)
r_i perimeter of vessel 'i' from the center of outer tissue cylinder $\{(a_{vi} + r_{vwi}\cos\theta_i)^2 + (r_{vwi}\sin\theta_i)^2\}^{\frac{1}{2}}$, $i = 1,2$ (m)
r_{vwi} radius of the ith vessel, $i = 1,2$ (m)
r_{tw} outer radius of the tissue boundary (m)
t temperature of the tissue
t_{avg} area averaged tissue matrix temperature, $\frac{1}{A_t}\int_{A_t} t\,dA$, (K)
$t_{vwi,1}$ mean temperature at the ith vessel wall, $i = 1,2$ (K)
$t_{vwi,2}$ fluctuation in temperature at the ith vessel wall, $i = 1,2$ (K)
$t_{tw,1}$ mean temperature at the tissue boundary (K)
$t_{tw,2}$ fluctuation in temperature at the tissue boundary (K)
x, y Cartesian coordinates in the original problem (m)
x_i, y_i Cartesian coordinates in sub-problem i, $x_1 = x,\ y_1 = y,\ x_2 = x_1\cos(\phi_1) + y_1\sin(\phi_1),\ y_2 = y_1\cos(\phi_1) - x_1\sin(\phi_1),\ i = 1,2\ (m)$

Non-dimensional parameters

A_{vi} distance between the centers of the tissue cylinder and the ith vessel, a_{vi}/r_{tw}, $i = 1,2$
a_{1i} constant for ith sub-problem, $A_{vi} - R_{vwi}$, $i = 1,2$
a_{2i} constant for ith sub-problem, $A_{vi} + R_{vwi}$, $i = 1,2$
A_{0i}, A'_{0i} constant associated with the solution of the ith sub-problem, $i = 1,2$
A_{ni}, A'_{ni} constant associated with the solution of the ith sub-problem, $i = 1,2$
B_{ni}, B'_{ni} constant associated with the solution of the ith sub-problem, $i = 1,2$
F_{vwi} temperature at vessel wall $i = 1,2$, $(f_{vwi} - t_{vw1,1})/(t_{vw,1} - t_{vw1,1})$
F_{tw} temperature at outer tissue boundary, $(f_{tw} - t_{vw1,1})/(t_{tw,1} - t_{vw1,1})$
n_{vwi} frequency of the temperature distribution at vessel i
P power deposition, $g'''r_{tw}^2/[(t_{tw,1} - t_{vw1,1})k]$
$Q_{vw2-vw1}$ heat transfer from vessel wall two to vessel wall one, $q_{vw2-vw1}/[(t_{tw,1} - t_{vw1,1})k]$
Q_{tw-vw1} heat transfer from tissue to vessel wall one, $q_{tw-vw1}/[(t_{tw,1} - t_{vw1,1})k]$
Q_{tw-vw2} heat transfer from tissue to vessel wall two, $q_{tw-vw2}/[(t_{tw,1} - t_{vw1,1})k]$
$Q_{total,vw1}$ total heat transfer into vessel wall one, $q_{total-vw1}/[(t_{tw,1} - t_{vw1,1})k]$
$Q_{total,vw2}$ total heat transfer into vessel wall two, $q_{total-vw2}/[(t_{tw,1} - t_{vw1,1})k]$
R radius, r/r_{tw}, $(X_1^2 + Y_1^2)^{1/2}$
R_i perimeter of vessel 'i' from the center of outer tissue cylinder $\{(A_{vi} + R_{vwi}\cos\theta_i)^2 + (R_{vwi}\sin\theta_i)^2\}^{1/2}$, $i = 1,2$ (m)
R_i^* radius in conformally mapped space for ith sub-problem, $(U_i^2 + V_i^2)^{1/2}$, $i = 1,2$
R_{vwi} radius of the ith vessel, r_{vwi}/r_{tw}, $i = 1,2$
S_{tw-vwi} PCSF defined based on the average tissue boundary and vessel wall temperatures to account for the heat transfer rate between vessel i and the tissue
S_{tm-vwi} PCSF defined based on the average tissue matrix and vessel wall temperatures to account for the heat transfer rate between vessel i and the tissue
$S_{vw1-vw2}$ PCSF defined based on the average vessel wall temperatures to account for the heat transfer between the two vessels
T temperature, $(t - t_{vw1,1})/(t_{tw,1} - t_{vw1,1})$
T_1 temperature, $T + PR^2/4$
T_{1i} temperature in sub-problem $i = 1,2$
U_i first of the two coordinates in the conformally mapped space that relates to the x and y coordinates of the original Cartesian coordinate system for ith sub-problem, $\{(X_i - \lambda_i)(1 - \lambda_i X_i) - \lambda_i Y_i^2\}/\{(1 - \lambda_i X_i)^2 - (\lambda_i Y_i)^2\}$, $i = 1,2$
V_i second of the two coordinates in the conformally mapped space that relates to the x and y coordinates of the original Cartesian coordinate system for ith sub-problem, $\{(1 - \lambda_i^2)Y_i\}/\{(1 - \lambda_i X_i)^2 - (\lambda_i Y_i)^2\}$, $i = 1,2$
w_i conformal transformation for ith sub-problem, $U_i + jV_i = (X_i + jY_i - \lambda_i)/(1 - \lambda_i(X_i + jY_i))$, $i = 1,2$

X_i, Y_i original Cartesian coordinate system in ith sub-problem $(x_i, y_i)/r_{tw}$, $i = 1, 2$

X_2 one of the two coordinates of sub-problem 2 related to the original coordinates and the coordinates of sub-problem 1, $X_1\cos(\phi_1) + Y_1\sin(\phi_1)$

Y_2 one of the two coordinates of sub-problem 2 related to the original coordinates and the coordinates of sub-problem 1, $Y_1\cos(\phi_1) - X_1\sin(\phi_1)$

Greek symbols

θ_i angular position from the center of the ith vessel in the original coordinate system, $i = 1, 2$

α_i angular position from the center of ith vessel in the transformed coordinate system, $\tan^{-1}(V_i/U_i)$, $i = 1, 2$

λ_i constant, $\{1 + a_{1i}a_{2i} - ((1 - a_{1i}^2)(1 - a_{2i}^2))^{1/2}\}/(a_{1i} + a_{2i})$, $i = 1, 2$

ψ angular position measured from the center of the tissue

ϕ_i angular position of center of the $(i + 1)$th vessel from the center of the tissue

ϕ_{vwi} phase angle of the temperature distribution at vessel i

applications such as thermoregulation and thermal therapy [8–20]. Thus a number of researchers have attempted to define and quantify the vessel–vessel and vessel–tissue heat transfer rates and the corresponding shape factors for the geometry of paired vessels in both infinite [8–10,12,15,21–23,28] and finite [11,14,17,18,24–27,29,30], and unheated [8–12,14,15,17,18,21–29] and heated [30] tissues. Several simplifications have been employed. First and the most important, only uniform boundary conditions with either constant and uniform Dirichlet (given temperature) boundary condition [8,9,12,14,15,21,23–25,28,30] or Robbins (convective) boundary condition with uniform and constant convective heat transfer coefficient and outer reference temperature [11,13,18,22,26,27,29] have been employed in all of the previous studies to estimate the heat transfer rates and shape factors. Since non-uniform boundary conditions are likely to be present on the vessel walls and any circular tissue boundary used to define shape factors in unheated and/or heated tissues due to various reasons (e.g., structure of the vessel network, non-uniform heating, etc.) [10,27], it is important to extend the previous derivations/studies to appropriately define/quantify/study the vessel–vessel and vessel–tissue heat transfer rates and the corresponding shape factors for the general case of non-uniform Dirichlet boundary conditions. Such an extended study will help an accurate quantification of the heat transfer rates and/or estimation of the variations in the heat transfer rates from the values estimated using only uniform boundary conditions in applications such as RF/microwave/ultrasound assisted hyperthermia, and high field MR imaging. In addition, a derivation is needed to evaluate the tissue temperature distribution in the geometry of arbitrarily located paired vessels in a heated tissue that allows independent specification of the general Dirichlet boundary conditions on all of the surfaces. Such derivations will facilitate the evaluation of the heat transfer rates and shape factors used in the development and implementation of improved bio-heat equations [e.g., 31].

Second, the effect of the externally induced tissue heating has been neglected in the explicit estimation of the vessel–vessel and vessel–tissue heat transfer rates in previous counter-current bio-heat transfer analyses except in [30]. Since the effect of external heating on the heat transfer rates is shown to be significant in several thermal therapy applications [30,32] (e.g., RF/microwave/ultrasound hyperthermia, high temperature cancer therapies, and high field MR imaging), a source term representing external heating is included in this study.

Third, in previous counter-current bio-heat transfer analyses (except in [30]) the evaluation of the vessel–vessel and vessel–tissue heat transfer rates and the corresponding shape factors is performed by assuming that the vessel–tissue heat transfer rates are zero, and/or the vessel–tissue heat transfer rates from the two vessels are equal to each other. The present analysis compliments the previous work by including the effect of unequal vessel–tissue heat transfer rates.

In summary, general Dirichlet boundary conditions are very likely to be present on vessel walls and outer tissue boundary because of the discrete arrangement of vessels in both, unheated/heated tissues. However, no study exists that appropriately defines and explicitly quantifies the vessel–vessel and vessel–tissue heat transfer rates and related shape factors for such boundary conditions—nor does an analytical derivation to facilitate the computation of these heat transfer rates and shape factors. Therefore, there are four major objectives of this study, to: (1) derive an analytical solution for the tissue temperature field that can be extended for the case of 3 closely spaced vessels [33]; (2) define and explicitly quantify the related vessel–vessel and vessel–tissue heat transfer rates; (3) define the corresponding shape factors, and; (4) study the effect of the boundary conditions on the heat transfer rates and these shape factors as a

function of various geometrical parameters in a finite tissue region with two arbitrarily located blood vessels and general Dirichlet boundary conditions. This work is an extension of our earlier work on the vessel–tissue thermal interactions with one vessel [32] with angularly varying tissue boundary/vessel wall temperatures and two vessels [30] with uniform tissue boundary/vessel wall temperatures. Additionally, note that by employing the approach developed by Klemick et al. [34] the newly developed 2D analytical solution can be extended to obtain an approximate 3D tissue temperature distribution.

2. Mathematical formulation

2.1. Solution

To meet the first objective, an exact, analytical series solution of the 2-D Poisson equation is developed for a finite, homogeneous, uniformly heated tissue region with two arbitrarily located circular vessels and non-uniform Dirichlet boundary conditions. A uniform source (which represents the summation of metabolic heating and the externally induced heating) distribution is assumed: (a) for simplicity, and (b) since the distribution of the source term can be approximated as being uniform over short distances for many heating systems whose power deposition patterns vary negligibly over distances of the magnitude of the tissue boundary radius. A source term similar to the Pennes' blood-tissue heat transfer related term [35] is not included in our model since it represents a method of replacing the effects of the vessels currently under study. In other words, the Pennes. blood-tissue heat transfer related term is an approximation of the cumulative blood-tissue heat transfer rate from the thermally significant vessels (vessels of diameter ~100–1000 μm) to tissue. Additionally, the vessels of diameter ~100–400 μm make the majority of the counter-current vessel pairs [33]. Since the goal of the paper is to explicitly quantify the vessel–vessel and vessel–tissue heat transfer rates in a tissue imbedded with a pair of thermally significant vessels, the Pennes' perfusion term is not included.

To obtain the temperature field we impose non-dimensional Eq. (1) in the tissue after converting it into a Laplace equation using the change of variable from T to T_1.

$$\frac{1}{R}\frac{\partial}{\partial R}\left(R\frac{\partial T_1}{\partial R}\right)+\frac{1}{R^2}\frac{\partial^2 T_1}{\partial \psi^2}=0 \tag{1}$$

The associated boundary conditions are (Fig. 1).

$$T_1|_{R_1}=F_{\mathrm{vw1}}(\theta_1)+PR_1^2/4 \tag{2}$$
$$T_1|_{R_2}=F_{\mathrm{vw2}}(\theta_2)+PR_2^2/4 \tag{3}$$
$$T_1|_1=F_{\mathrm{tw}}(\psi)+P|4 \tag{4}$$

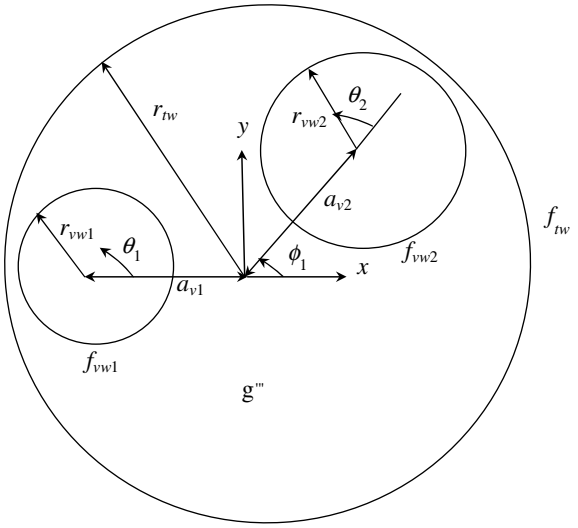

Fig. 1. Schematic of the tissue cylinder with two unequal arbitrarily located vessels.

The problem defined above can be rewritten as the superposition of two sub-problems:

Sub-problem A-1:

$$\frac{1}{R}\frac{\partial}{\partial R}\left(R\frac{\partial T_{11}}{\partial R}\right)+\frac{1}{R^2}\frac{\partial^2 T_{11}}{\partial \psi^2}=0 \tag{5}$$
$$T_{11}|_{R_1}=F_{\mathrm{vw1}}(\theta_1)+PR_1^2/4-c_{21} \tag{6}$$
$$T_{11}|_{R_2}=c_{12} \tag{7}$$
$$T_{11}|_1=F_{\mathrm{tw}}(\psi)+P/4 \tag{8}$$

Sub-problem A-2:

$$\frac{1}{R}\frac{\partial}{\partial R}\left(R\frac{\partial T_{12}}{\partial R}\right)+\frac{1}{R^2}\frac{\partial^2 T_{12}}{\partial \psi^2}=0 \tag{9}$$
$$T_{12}|_{R_1}=c_{21} \tag{10}$$
$$T_{12}|_{R_2}=F_{\mathrm{vw2}}(\theta_2)+PR_2^2/4-c_{12} \tag{11}$$
$$T_{12}|_1=0 \tag{12}$$

where,

$$T_1=T_{11}+T_{12} \tag{13}$$

This division allows us to rewrite the original problem with two blood vessels as a summation of two sub-problems each consisting of only one of the two vessels. Here, c_{ij} is the temperature distribution produced on the wall of the jth vessel by the wall of the ith vessel in sub-problem i. Note, that the values of the c_{ij} are not known and therefore the boundary conditions (6), (7), (10), and (11) cannot be used to obtain the complete solution–this issue has been addressed later in the paper. To simplify the problem even further by making the vessel and the

tissue concentric [36] in both sub-problems, standard bilinear transformation (w_i) is used. The modified sub-problem A-1 with boundary condition Eq. (8) can be written as

$$\frac{1}{R_1^*}\frac{\partial}{\partial R_1^*}\left(R_1^*\frac{\partial T_{11}}{\partial R_1^*}\right)+\frac{1}{(R_1^*)^2}\frac{\partial^2 T_{11}}{\partial \alpha_1^2}=0 \tag{14}$$

with,

$$T_{11}|_1 = F_{\mathrm{tw}}(\psi)+P/4 \tag{15}$$

The general solution to Eq. (14) is [37]:

$$\begin{aligned}T_{11} &= A_{01}+A'_{01}\ln(R_1^*)+\sum_{n=1}^{\infty}\{A_{n1}(R_1^*)^n\\ &\quad + A'_{n1}(R_1^*)^{-n}\}\sin(n\alpha_1)+\sum_{n=1}^{\infty}\{B_{n1}(R_1^*)^n\\ &\quad + B'_{n1}(R_1^*)^{-n}\}\cos(n\alpha_1)\end{aligned} \tag{16}$$

Using Eqs. (15) and (16) and the orthogonality of sine and cosine functions, the following relations can easily be derived:

$$A_{01}=\frac{1}{2\pi}\int_0^{2\pi}F_{\mathrm{tw}}(\psi(U_1,V_1))\,\mathrm{d}\alpha_1+P/4 \tag{17}$$

$$\begin{aligned}A_{n1}+A'_{n1}=S_{A_{n1}} &= \frac{1}{\pi}\int_0^{2\pi}F_{\mathrm{tw}}(\psi(U_1,V_1))\\ &\quad\times\sin(n\alpha_1)\,\mathrm{d}\alpha_1\end{aligned} \tag{18}$$

$$\begin{aligned}B_{n1}+B'_{n1}=S_{B_{n1}} &= \frac{1}{\pi}\int_0^{2\pi}F_{\mathrm{tw}}(\psi(U_1,V_1))\\ &\quad\times\cos(n\alpha_1)\,\mathrm{d}\alpha_1\end{aligned} \tag{19}$$

Using Eqs. (17)–(19), Eq. (16) can be rewritten as follows:

$$\begin{aligned}T_{11} &= A_{01}+A'_{01}\ln(R_1^*)\\ &\quad+\sum_{n=1}^{\infty}A_{n1}\{(R_1^*)^n-(R_1^*)^{-n}\}\sin(n\alpha_1)\\ &\quad+\sum_{n=1}^{\infty}S_{A_{n1}}(R_1^*)^{-n}\sin(n\alpha_1)\\ &\quad+\sum_{n=1}^{\infty}B_{n1}\{(R_1^*)^n-(R_1^*)^{-n}\}\cos(n\alpha_1)\\ &\quad+\sum_{n=1}^{\infty}S_{B_{n1}}(R_1^*)^{-n}\cos(n\alpha_1)\end{aligned} \tag{20}$$

Similarly, for sub-problem A-2, the following solution can be obtained after applying the transformation w_2 that makes vessel two and tissue concentric and the boundary condition at the tissue boundary Eq. (12) in the transformed plane:

$$\begin{aligned}T_{12} &= A'_{02}\ln(R_2^*)+\sum_{n=1}^{\infty}A_{n2}\{(R_2^*)^n-(R_2^*)^{-n}\}\sin(n\alpha_2)\\ &\quad+\sum_{n=1}^{\infty}B_{n2}\{(R_2^*)^n-(R_2^*)^{-n}\}\cos(n\alpha_2)\end{aligned} \tag{21}$$

The complete solution using Eq. (13) and transforming variable T_1 back to T, can be written as

$$\begin{aligned}T &= A_{01}+A'_{01}\ln(R_1^*)+A'_{02}\ln(R_2^*)\\ &\quad+\sum_{n=1}^{\infty}A_{n1}\{(R_1^*)^n-(R_1^*)^{-n}\}\sin(n\alpha_1)\\ &\quad+\sum_{n=1}^{\infty}A_{n2}\{(R_2^*)^n-(R_2^*)^{-n}\}\sin(n\alpha_2)\\ &\quad+\sum_{n=1}^{\infty}B_{n1}\{(R_1^*)^n-(R_1^*)^{-n}\}\cos(n\alpha_1)\\ &\quad+\sum_{n=1}^{\infty}B_{n2}\{(R_2^*)^n-(R_2^*)^{-n}\}\cos(n\alpha_2)\\ &\quad+\sum_{n=1}^{\infty}S_{A_{n1}}(R_1^*)^{-n}\sin(n\alpha_1)\\ &\quad+\sum_{n=1}^{\infty}S_{B_{n1}}(R_1^*)^{-n}\cos(n\alpha_1)-PR^2/4\end{aligned} \tag{22}$$

As mentioned above, since the values of c_{ij} in Eqs. (6), (7), (10), and (11) are not known, the constants presented in Eq. (22) cannot be evaluated in the transformed plane. Therefore, to evaluate all of the constants (A'_{01}, A'_{02}, A'_{n1}, A'_{n2}, B'_{n1} and B'_{n2}), the expression shown in Eq. (22) should be expressed in the original coordinates using relationships presented in the nomenclature section that relate R, R_1^*, α_1, R_2^*, and α_2 to the original coordinates X_1 and Y_1 since the vessel wall boundary conditions are known in the original plane (given temperatures). To evaluate the complete set of $2(2N+1)$ constants where N is the finite number of terms considered in each of the above summation series, a system of $2(2N+1)$ independent linear equations consisting of $2(2N+1)$ constants should be formed by multiplying the boundary condition equation $(i+1)$ and the solution Eq. (22) with $\sin(m\theta_i)$ and $\cos(m\theta_i)(m=0,\ldots,N)$, respectively, and integrating over the perimeter of the ith vessel ($i=1,2$) (Appendix A). The obtained system of two $(2N+1)$ linear equations (due to two vessel wall boundary conditions) with $2(2N+1)$ constants can be evaluated using any linear equation solver. It can also be realized from the above description that every other addition of a vessel in the finite tissue medium introduces, in general, another $(2N+1)$ constants, which can be evaluated using the additional vessel wall boundary conditions. The new, 2D, non-dimensional solution is valid for large vessels (i.e., vessels of diameter $\geqslant 1$ mm) also, provided the tissue heating around them can be considered as uniform.

2.2. Heat transfer rates

To meet the goal of appropriately defining and quantifying the vessel–vessel and vessel–tissue heat transfer

rates it is important to account for the fact that in a finite, non-insulated tissue with two vessels, some of the energy leaving each vessel wall goes to the other vessel wall and the rest of it goes to the outer tissue boundary. We can express this physical situation as follows:

$$Q_{\text{total,vw1}} = Q_{\text{vw2–vw1}} + Q_{\text{tw–vw1}} \tag{23}$$

$$Q_{\text{total,vw2}} = Q_{\text{vw1–vw2}} + Q_{\text{tw–vw2}} \tag{24}$$

Further, using the exact solution for the tissue temperature field presented in the previous section the total heat transfer rate entering each vessel wall can be calculated by evaluating and integrating the flux around the vessels. Thus in order to evaluate the vessel–vessel and vessel–tissue heat transfer rates in the original problem (Fig. 1), we have only two equations, Eqs. (23) and (24), and four unknown heat fluxes (i.e., $Q_{\text{vw2–vw1}}$, $Q_{\text{tw–vw1}}$, $Q_{\text{vw1–vw2}}$, $Q_{\text{tw–vw2}}$). (Note that in our evaluation we do not assume, that $Q_{\text{vw2–vw1}} = Q_{\text{vw1–vw2}}$, but rather we will evaluate each of these terms separately.) To obtain the needed additional expressions to explicitly evaluate these heat transfer rates, the original problem (Fig. 1) is presented as the superposition of the following two sub-problems–one, with no tissue heating, zero outer tissue boundary temperature and the given fluctuations at the vessel walls (sub-problem B-1), and the other, with the tissue heating, given fluctuations at the outer tissue boundary and zero temperatures at the vessel walls (sub-problem B-2). Hypothesizing that there is no heat transfer rate between the surfaces with zero temperatures irrespective of the tissue temperature distribution in between those two surfaces (we will prove this hypothesis shortly), equations for the heat transfer rates for the first sub-problem can be written as follows.

For sub-problem B-1:

$$(Q_{\text{total,vw1}})_{\text{B-1}} = (Q_{\text{vw2–vw1}})_{\text{B-1}} + (Q_{\text{tw–vw1}})_{\text{B-1}} \tag{25}$$

$$(Q_{\text{total,vw2}})_{\text{B-1}} = (Q_{\text{vw1–vw2}})_{\text{B-1}} + (Q_{\text{tw–vw2}})_{\text{B-1}} \tag{26}$$

To prove our hypothesis, the sub-problem B-1 is further sub-divided into two other sub-sub-problems; the first with the fluctuations on vessel wall one and zero temperatures at the other boundaries (sub-sub-problem B-1-1), and the second with the fluctuations on vessel wall two and zero temperatures at the other boundaries (sub-sub-problem B-1-2). If and if only our hypothesis is correct, can the equations for the heat transfer rates in these sub-sub-problems be written as below.

For sub-sub-problem B-1-1:

$$(Q_{\text{total,tb}})_{\text{B-1-1}} = (Q_{\text{tw–vw1}})_{\text{B-1}} \tag{27}$$

For sub-sub-problem B-1-2:

$$(Q_{\text{total,tb}})_{\text{B-1-2}} = (Q_{\text{tw–vw2}})_{\text{B-1}} \tag{28}$$

Eqs. (27) and (28) show that evaluating and integrating the flux around the tissue boundary in sub-sub-problems B-1-1 and B-1-2 would provide the vessel–tissue heat transfer rates from vessels one and two, respectively, for sub-problem B-1. Subtracting these vessel–tissue heat transfer rates from the total vessel heat transfer rates, presented in Eqs. (25) and (26), would provide evaluation of the vessel one to vessel two ($(Q_{\text{vw1–vw2}})_{\text{B-1}}$) and from vessel two to vessel one ($(Q_{\text{vw1–vw2}})_{\text{B-1}}$) heat transfer rates for sub-problem B-1. Since we know that the vessel–vessel heat transfer rates should be equal in magnitude and opposite in sign for any arbitrary temperature distribution at the two vessel walls and outer tissue boundary, it should be so in the evaluations of ($(Q_{\text{vw1–vw2}})_{\text{B-1}}$) and ($(Q_{\text{vw2–vw1}})_{\text{B-1}}$) to independently validate our hypothesis. As is presented later in the results section, we have found that the two vessel–vessel heat transfer rates were equal to each other and opposite in signs for all the cases studied herein, thus verifying the hypothesis that there is no heat transfer rate between the surfaces with zero temperatures.

Now, in accordance with our proven hypothesis, the second sub-problem B-2 does not result in any vessel–vessel heat transfer rate (the vessel wall temperatures are zero) and therefore, the original vessel–vessel heat transfer rate, present in Fig. 1, is completely contained in the first sub-problem B-1. Therefore the vessel–vessel heat transfer rates quantified for the first sub-problem are the vessel–vessel heat transfer rates present in the original problem. Once, the vessel–vessel heat transfer rate is known, the vessel–tissue heat transfer rates can be evaluated using Eqs. (23) and (24).

2.3. Poisson conduction shape factors

Once the heat transfer rates are determined, the third objective of the paper is fulfilled by defining the vessel–vessel and vessel–tissue Poisson conduction shape factors based on the average vessel wall temperatures and the average tissue boundary temperature. These expressions in their non-dimensional form, for the unit length of the tissue cylinder, are presented as follows:

$$Q_{\text{total,vw1}} = S_{\text{vw2–vw1}}(T_{\text{vw2,1}} - T_{\text{vw1,1}}) + S_{\text{tw–vw1}}(T_{\text{tw,1}} - T_{\text{vw1,1}}) \tag{29}$$

$$Q_{\text{total,vw2}} = S_{\text{vw2–vw1}}(T_{\text{vw1,1}} - T_{\text{vw2,1}}) + S_{\text{tw–vw2}}(T_{\text{tw,1}} - T_{\text{vw2,1}}) \tag{30}$$

Alternatively, based on the average vessel wall temperatures and the average tissue matrix temperature, the two VTPCSFs can be defined as follows (again, equations are presented in their no-dimensional form):

$$Q_{\text{total,vw1}} = S_{\text{vw2–vw1}}(T_{\text{vw2,1}} - T_{\text{vw1,1}}) + S_{\text{tm–vw1}}(T_{\text{avg}} - T_{\text{vw1,1}}) \tag{31}$$

$$Q_{\text{total,vw2}} = S_{\text{vw2–vw1}}(T_{\text{vw1,1}} - T_{\text{vw2,1}}) + S_{\text{tm–vw2}}(T_{\text{avg}} - T_{\text{vw2,1}}) \tag{32}$$

2.4. Parametric solutions

To meet the last objective of this study, i.e., to study the effect of boundary conditions on the heat transfer rates and the corresponding shape factors in heated, finite tissues for a particular case of biological interest, the cosine variations in Eqs. (33)–(35) are used since (1) Wissler [10] has shown that for two nearby vessels in an infinite unheated tissue matrix, the angular variation in vessel wall temperature is similar to a cosine function, and (2) any continuous temperature variation on the vessel walls and outer tissue boundary can be represented as a Fourier series with a summation of an average, non-fluctuating value and a series of sines and cosines with zero mean temperature. (Only one of the terms in this series of sines and cosines has been studied since (1) the physics of the problem does not change if we consider more terms, and (2) if the results with additional terms are desired the effect of other sine and cosine terms on the tissue temperature distribution, heat transfer rates, and the shape factors can be superimposed on the present results due to the linearity of the problem.)

$$F_{\mathrm{vw1}}(\theta_1) = 0 + T_{\mathrm{vw1,2}}\cos(n_{\mathrm{vw1}}\theta_1 + \phi_{\mathrm{vw1}}) \tag{33}$$

$$F_{\mathrm{vw2}}(\theta_1) = T_{\mathrm{vw2,1}} + T_{\mathrm{vw2,2}}\cos(n_{\mathrm{vw2}}\theta_2 + \phi_{\mathrm{vw2}}) \tag{34}$$

$$F_{\mathrm{tw}}(\psi) = 1 + T_{\mathrm{tw,2}}\cos(n_{\mathrm{tw}}\psi + \phi_{\mathrm{tw}}) \tag{35}$$

We studied the effects of the fluctuations at the vessel wall two on the heat transfer rates and PCSFs as a function of the geometrical parameters for the typical case of cold vessels [12,41,42], i.e., when the average tissue boundary temperature is higher than the average vessel wall temperatures [38]. To perform the parametric study, different fluctuation parameters in Eq. (34) are varied one at a time by keeping the vessel one's wall temperature and the tissue boundary temperature fixed. Different values are assigned in Eq. (34) between: 0 and 1 for the magnitudes of fluctuations ($T_{\mathrm{vw2,2}}$) (which corresponds to ±5 °C) [39–41]; 0 and π for the phase angles (ϕ_{vw2}), i.e., by rotating the imposed temperature fields (simulating non-uniform tissue temperature distribution), and 0 and 3 for n_{vw2}, i.e., by varying the number of the imposed fluctuation peaks (simulating non-uniform tissue temperature distribution) (Figs. 3–11). While all of the results are presented in Devashish [38], the current study presents only the results for the effects of vessel two's wall temperature fluctuations on the PCSFs defined based on the average tissue boundary temperature. The effects of these fluctuations on the average tissue matrix based PCSFs are not presented since those results are similar to the results for the average tissue boundary temperature based PCSFs [38].

Further, to study a general case of unequal vessel wall temperatures it is assumed in our study that the

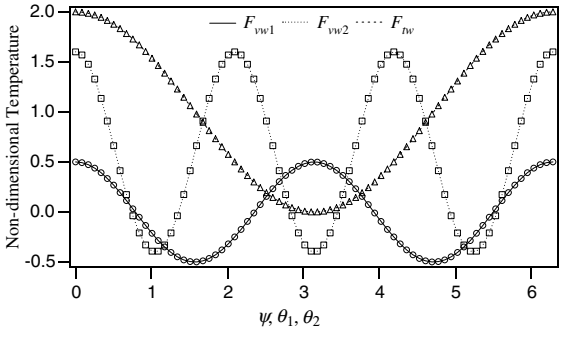

Fig. 2. Validity of the solution is presented for $N = 20$, $P = 50$, $R_{\mathrm{vw1}} = 0.2$, $A_{\mathrm{v1}} = -0.6$, $T_{\mathrm{vw1,1}} = 0.0$, $T_{\mathrm{vw1,2}} = 0.5$, $n_{\mathrm{vw1}} = 2$, $\phi_{\mathrm{vw1}} = 0$, $R_{\mathrm{vw2}} = A_{\mathrm{v2}} = 0.3$, $T_{\mathrm{vw2,1}} = 0.6$, $T_{\mathrm{vw2,2}} = 1.0$, $n_{\mathrm{vw2}} = 3$, $\phi_{\mathrm{vw2}} = 0$, $T_{\mathrm{tw,1}} = 1.0$, $t_{\mathrm{tw,2}} = 1.0$, $n_{\mathrm{tw}} = 1$, $\phi_{\mathrm{tw}} = 0$. Lines and markers represent the given and evaluated boundary conditions, respectively, at the two vessel walls and outer tissue boundary.

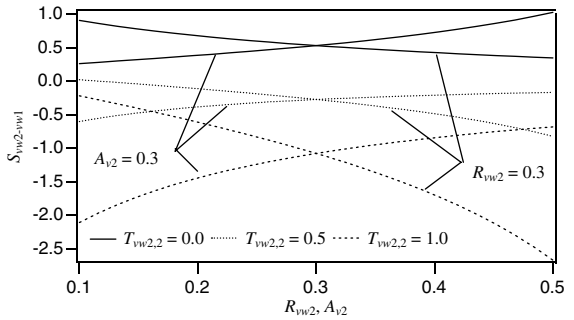

Fig. 3. Effect of the magnitude of the fluctuation at vessel wall two on the vessel–vessel Poisson conduction shape factor vs. the vessel two radius and eccentricity for: $N = 20$, $P = 50$, $R_{\mathrm{vw1}} = 0.2$, $A_{\mathrm{v1}} = -0.6$, $T_{\mathrm{vw1,1}} = 0.0$, $T_{\mathrm{vw1,2}} = 0.5$, $n_{\mathrm{vw1}} = 1$, $\phi_{\mathrm{vw1}} = 0$, $T_{\mathrm{vw2,1}} = 0.6$, $n_{\mathrm{vw2}} = 1$, $\phi_{\mathrm{vw2}} = 0$, $T_{\mathrm{tw,1}} = 1.0$, $T_{\mathrm{tw,2}} = 1.0$, $n_{\mathrm{tw}} = 1$, $\phi_{\mathrm{tw}} = 0$.

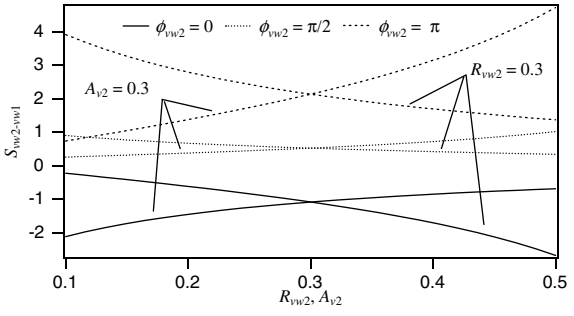

Fig. 4. Effect of the phase of the fluctuation at vessel wall two on the vessel–vessel Poisson conduction shape factor vs. the vessel two radius and eccentricity for: $N = 20$, $P = 50$, $R_{\mathrm{vw1}} = 0.2$, $A_{\mathrm{v1}} = -0.6$, $T_{\mathrm{vw1,1}} = 0.0$, $T_{\mathrm{vw1,2}} = 0.5$, $n_{\mathrm{vw1}} = 1$, $\phi_{\mathrm{vw1}} = 0$, $T_{\mathrm{vw2,1}} = 0.6$, $T_{\mathrm{vw2,2}} = 1.0$, $n_{\mathrm{vw2}} = 1$, $T_{\mathrm{tw,1}} = 1.0$, $T_{\mathrm{tw,2}} = 1.0$, $n_{\mathrm{tw}} = 1$, $\phi_{\mathrm{tw}} = 0$.

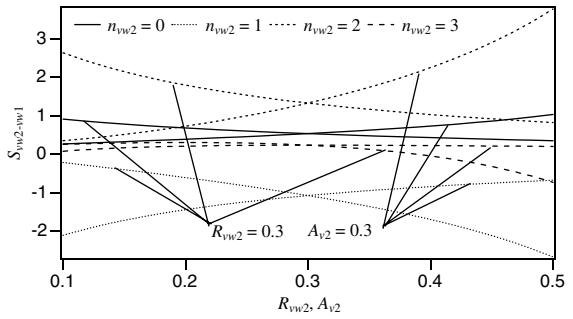

Fig. 5. Effect of the frequency of the fluctuation at vessel wall two on the vessel–vessel Poisson conduction shape factor vs. the vessel two radius and eccentricity for: $N = 20$, $P = 50$, $R_{vw1} = 0.2$, $A_{v1} = -0.6$, $T_{vw1,1} = 0.0$, $T_{vw1,2} = 0.5$, $n_{vw1} = 1$, $\phi_{vw1} = 0$, $T_{vw2,1} = 0.6$, $T_{vw2,2} = 1.0$, $\phi_{vw2} = 0$, $T_{tw,1} = 1.0$, $T_{tw,2} = 1.0$, $n_{tw} = 1$, $\phi_{tw} = 0$.

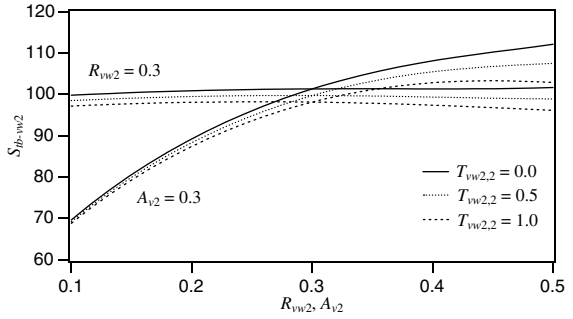

Fig. 6. Effect of the magnitude of the fluctuation at vessel wall two on the vessel two's vessel–tissue Poisson conduction shape factor vs. the vessel two radius and eccentricity for: $N = 20$, $P = 50$, $R_{vw1} = 0.2$, $A_{v1} = -0.6$, $T_{vw1,1} = 0.0$, $T_{vw1,2} = 0.5$, $n_{vw1} = 1$, $\phi_{vw1} = 0$, $T_{vw2,1} = 0.6$, $n_{vw2} = 1$, $\phi_{vw2} = 0$, $T_{tw,1} = 1.0$, $T_{tw,2} = 1.0$, $n_{tw} = 1$, $\phi_{tw} = 0$.

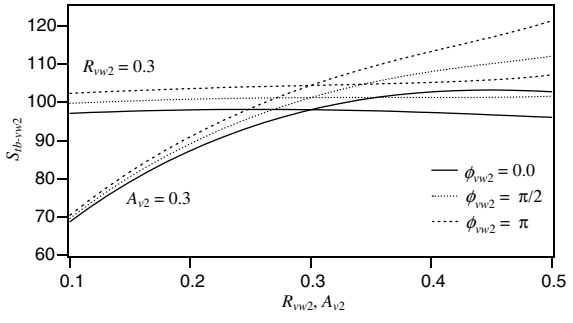

Fig. 7. Effect of the phase of the fluctuation at vessel wall two on the vessel two's vessel–tissue Poisson conduction shape factor vs. the vessel two radius and eccentricity for: $N = 20$, $P = 50$, $R_{vw1} = 0.2$, $A_{v1} = -0.6$, $T_{vw1,1} = 0.0$, $T_{vw1,2} = 0.5$, $n_{vw1} = 1$, $\phi_{vw1} = 0$, $T_{vw2,1} = 0.6$, $T_{vw2,2} = 1.0$, $n_{vw2} = 1$, $T_{tw,1} = 1.0$, $T_{tw,2} = 1.0$, $n_{tw} = 1$, $\phi_{tw} = 0$.

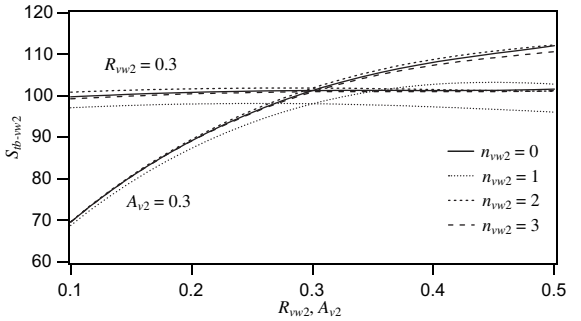

Fig. 8. Effect of the frequency of the fluctuation at vessel wall two on the vessel two's vessel–tissue Poisson conduction shape factor vs. the vessel two radius and eccentricity for: $N = 20$, $P = 50$, $R_{vw1} = 0.2$, $A_{v1} = -0.6$, $T_{vw1,1} = 0.0$, $T_{vw1,2} = 0.5$, $n_{vw1} = 1$, $\phi_{vw1} = 0$, $T_{vw2,1} = 0.6$, $T_{vw2,2} = 1.0$, $\phi_{vw2} = 0$, $T_{tw,1} = 1.0$, $T_{tw,2} = 1.0$, $n_{tw} = 1$, $\phi_{tw} = 0$.

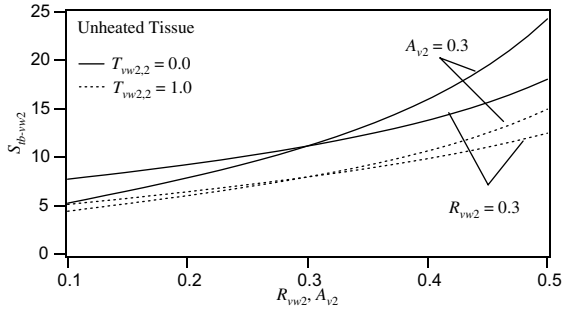

Fig. 9. Effect of the magnitude of the fluctuation at vessel wall two on the vessel two's vessel–tissue Poisson conduction shape factor vs. the vessel two radius and eccentricity for: $N = 20$, $P = 0$, $R_{vw1} = 0.2$, $A_{v1} = -0.6$, $T_{vw1,1} = 0.0$, $T_{vw1,2} = 0.5$, $n_{vw1} = 1$, $\phi_{vw1} = 0$, $T_{vw2,1} = 0.6$, $n_{vw2} = 1$, $\phi_{vw2} = 0$, $T_{tw,1} = 1.0$, $T_{tw,2} = 1.0$, $n_{tw} = 1$, $\phi_{tw} = 0$.

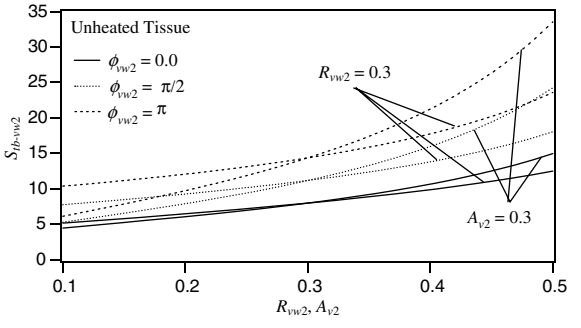

Fig. 10. Effect of the phase of the fluctuation at vessel wall two on the vessel two's vessel–tissue Poisson conduction shape factor vs. the vessel two radius and eccentricity for: $N = 20$, $P = 0$, $R_{vw1} = 0.2$, $A_{v1} = -0.6$, $T_{vw1,1} = 0.0$, $T_{vw1,2} = 0.5$, $n_{vw1} = 1$, $\phi_{vw1} = 0$, $T_{vw2,1} = 0.6$, $T_{vw2,2} = 1.0$, $n_{vw2} = 1$, $T_{tw,1} = 1.0$, $T_{tw,2} = 1.0$, $n_{tw} = 1$, $\phi_{tw} = 0$.

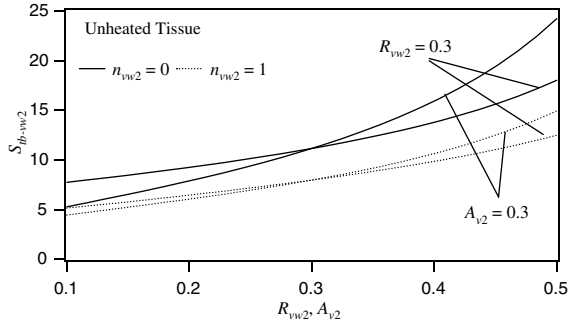

Fig. 11. Effect of the frequency of the fluctuation at vessel wall two on the vessel two's vessel–tissue Poisson conduction shape factor vs. the vessel two radius and eccentricity for: $N = 20$, $P = 50$, $R_{vw1} = 0.2$, $A_{v1} = -0.6$, $T_{vw1,1} = 0.0$, $T_{vw1,2} = 0.5$, $n_{vw1} = 1$, $\phi_{vw1} = 0$, $T_{vw2,1} = 0.6$, $T_{vw2,2} = 1.0$, $\phi_{vw2} = 0$, $T_{tw,1} = 1.0$, $T_{tw,2} = 1.0$, $n_{tw} = 1$, $\phi_{tw} = 0$.

average wall temperature of vessel two (simulating a vein) is higher than the average wall temperature of vessel one (simulating an artery) and is approximately half way ($T_{vw2,1} = 0.6$) in between the average wall temperatures of vessel one and outer tissue boundary. Also, since in high temperature therapy applications the temperature of the vessel wall and the tissue boundary usually varies in between 38 °C and 43 °C, this gives the average vessel two wall temperature of 41 °C [39–41] which is reasonable since arteries bring in cooler blood to the heated tissues from rest of the body and veins take out warmer blood from the heated arteries and veins. Since the average tissue matrix temperature reaches at least 43 °C [39–41], the non-dimensional source term P, which is the summation of the metabolic heat generation and externally induced heating, takes the maximum value of 50 in Figs. 3–8 so that the difference between the area averaged tissue matrix temperature and the average vessel wall one temperature reaches approximately two times the difference between the average tissue boundary and vessel wall one temperatures. To study the effect of the source term on the vessel–tissue heat transfer rates and VTPCSFs, the results are also presented for the unheated tissues (Figs. 9–11). The total number of terms 'N' used in the series solution to produce results is 20. This makes the maximum error in the evaluation of boundary temperatures (Fig. 2) less than 0.5%, which is sufficient for bio-heat transfer applications [27].

Next, regarding the rationale behind assigning specific values to geometrical parameters, this is given in [30] and is as follows. Since it is well known that the vessels of radius ~50–200 μm are thermally significant and make the majority of the counter-current vessel pairs [33,43], and the ratio of diameters of veins to arteries in living systems varies from ~1 to 2 [7,44,45], to study the effect of the vessel radius on the heat transfer rates and PCSFs, the non-dimensional radius of vessel two, R_{vw2} is varied from 0.1 to 0.5 (~56–282 μm) while keeping the non-dimensional radius of vessel one as 0.2 (~112 μm) and assuming that the radius of the tissue matrix is ~564 μm (since there are 1–3 vessels in the tissue of the size of 1 mm^2 [33]). The value of the eccentricity of vessel one, A_{v1} is chosen as −0.6 and the value of vessel two's eccentricity, A_{v2} is chosen as +0.3 to be able to put part of the perimeter of the vessels close to the tissue boundary to see the boundary effects. To study the effect of the vessel eccentricity on the heat transfer rates and PCSFs in the cases of traditional vessel pairs [33] (when the smallest distance between the two vessel walls is not greater than the largest diameter of the two vessels), the eccentricity of vessel two is varied from 0.1 to 0.5. The non-dimensional eccentricity of vessel one is kept as −0.6 for the afore mentioned reasons. The non-dimensional radii of vessels one and two are chosen as 0.2 and 0.3 respectively, since, as mentioned before, the ratio of the diameters of the veins to arteries varies in between 1 and 2 in living systems [7,44,45].

3. Results

First, in terms of model verification it was found that the two vessel–vessel heat transfer rate terms, $Q_{vw1-vw2}$ and $Q_{vw2-vw1}$ are always equal to each other in magnitude and opposite in sign for all vessel diameters, eccentricities, and wall temperatures studied. These results verify our hypothesis that there is no heat transfer rate between the surfaces with zero temperatures irrespective of the tissue temperature field in between them. Additionally, Fig. 2 presents the given and calculated boundary conditions for the heated tissue case to show that the developed solution satisfies all the boundary conditions and thus validating our solution further.

In terms of specific results, Figs. 3–5 present the variation in the VVPCSFs with the non-dimensional vessel two radius (R_{vw2}) and eccentricity (A_{v2}) for different values of the vessel two fluctuation parameters $T_{vw2,2}$, ϕ_{vw2}, and n_{vw2}. Notice that these results are valid for both, unheated and heated tissues since source term does not affect the vessel–vessel heat transfer rate and the VVPCSF. Further, since the VVPCSFs are a scaled measure of the non-dimensional vessel–vessel heat transfer rate ($Q_{vw1-vw2}$), thus the results in Figs. 3–5 can also be thought of as curves for $Q_{vw1-vw2}$ [30].

To compare with the results presented in Figs. 3–5 for the VVPCSFs and also to study the effects of the fluctuations on the vessel two to tissue heat transfer rates, Figs. 6–8 present the variation in the VTPCSFs for heated tissues ($P = 50$) with the non-dimensional vessel two radius (R_{vw2}) and eccentricity (A_{v2}) for different values of the fluctuation parameters $T_{vw2,2}$, ϕ_{vw2}, and n_{vw2}, respectively. In addition, since the VTPCSFs are

a scaled measure of the non-dimensional vessel–tissue heat transfer rate (Q_{tw-vw2}) thus the results in Figs. 6–8 can also be thought of as curves for Q_{tw-vw2}.

To study the effect of power and also to show how the effects of fluctuations increase in mildly heated tissue, Figs. 9–11 present the variation in the VTPCSFs for unheated tissues ($P = 0$) with the non-dimensional vessel two radius (R_{vw2}) and eccentricity (A_{v2}) for different values of the fluctuation parameters $T_{vw2,2}$, ϕ_{vw2}, and n_{vw2}.

4. Discussion

The goal of our work was to appropriately define and explicitly quantify the vessel–vessel and vessel–tissue heat transfer rates and the associated Poisson conduction shape factors when spatially variable boundary conditions are present. The first, and most important result is that the vessel–vessel heat transfer rates and the related shape factors significantly depend on the magnitude (Fig. 3), phase (Fig. 4) and frequency (Fig. 5) of the vessel wall temperature fluctuations. They do not, however, depend on the tissue boundary temperature fluctuations and/or the source term. This result is easily explained by noticing that the vessel–vessel heat transfer rate is contained in the sub-problem B-1 which is unaffected by the sub-problem B-2 containing the tissue boundary temperature fluctuations and the source term. It is significant that even though the average temperature of vessel wall two is higher than the average temperature of vessel wall one in all of the cases in Figs. 3–5, the presence of (zero mean) fluctuations can reverse vessel–vessel heat transfer direction and cause energy to flow from vessel wall one to two- instead of from vessel two to vessel one, as traditionally would be thought and modeled. This can easily be explained by realizing that the vessel–vessel heat transfer rates and thus the vessel–vessel Poisson conduction shape factors are significantly affected by the temperature distribution at the parts of the two vessel perimeters that are close to each other (Figs. 3–5). Since, the vessel–vessel heat transfer is an important mechanism in thermoregulation, our first result suggests the importance of including the effects of fluctuations in modeling this heat transfer rate.

Second, similar to the vessel–vessel heat transfer rates and VVPCSFs, the vessel–tissue heat transfer rates and the relevant shape factors also depend on the vessel wall temperature fluctuations (Figs. 6–11). This result can easily be explained by noticing that in sub-problem B-1, the fluctuations on the vessel walls will change the temperature difference between these vessels and the outer tissue boundary and thus will affect the net heat transfer rate between the tissue and the vessels. The effect of the tissue boundary temperature fluctuations on the vessel–tissue heat transfer rate will also be significant as can be explained from sub-problem B-2. Additionally, realize that the vessel 2–tissue heat transfer rate and thus the vessel 2–tissue Poisson conduction shape factor are significantly affected by the temperature distribution at the parts of the vessel 2 and outer tissue boundary perimeters that are close to each other. Further, the effect of the vessel wall fluctuations on the vessel to tissue heat transfer rates decreases as the strength of the source term increases (Figs. 9–11). This can be explained since an increase in the strength of the source term increases the heat transfer rates from tissue to vessels (sub-problem B-2) without affecting the heat transfer rates due to fluctuations.

Third, regarding the definition of shape factors, it can be noticed from sub-problem B-2 that although there is a finite heat transfer rate between the tissue and the vessels, the average temperature difference between any two surfaces is zero. Similarly, if sub-problem 3-1 is divided in two sub-sub-problems; one, with the average temperatures and the other with the fluctuations only, the second sub-sub-problem has a finite heat transfer rate between the two vessel walls and between the vessel walls and the tissue boundary, with zero average temperature difference between any two surfaces. Therefore, the average vessel wall and tissue boundary temperatures based shape factors are singular for these problems. Further, it can be seen from Eqs. (31) and (32) that the average tissue matrix based shape factors also have the potential to approach infinity if this temperature approaches any of the two average vessel wall temperatures. These observations suggest that new definitions of shape factors are needed that are bounded.

Fourth, again regarding the definition of shape factors, since in sub-problem B-2 there is a finite heat transfer rate between the vessel walls and outer tissue boundary which is, in general, not proportional to the average temperature difference between the two surfaces (or between the average tissue matrix temperature and the vessel wall temperatures), the shape factors are functions of the boundary temperatures themselves.

Fifth, it can be realized from Figs. 6–11 that the vessel–tissue heat transfer rates from vessel two is dependent on the fluctuations, while the vessel one to tissue heat transfer rate is fixed (since the temperature difference between those two surfaces is fixed). Thus, in general, the vessel–tissue heat transfer rates are neither equal to each other nor is their summation zero. Therefore, the vessel–vessel heat transfer analyses that include the assumption that there is no net vessels to tissue heat transfer [8,9,12,15,21–23,28], or that the vessel to tissue heat transfer rates are equal to each other [8,11,12,14,18,24–27,29], or that there is no vessel–vessel heat transfer [17] have limited applicability in principle, and the limits of their usefulness need to be evaluated.

Regarding the limitations of this study, although the present study gives useful insights into the quantitative

behavior of the heat transfer rates and the shape factors in 2-D, it neglects the effect of axial tissue conduction. In order to have more realistic estimates of the heat transfer rates and the shape factors the present study should be extended to 3-D geometries with general Dirichlet boundary conditions.

5. Conclusions

This paper presents an exact analytical series solution for the tissue temperature distribution in a finite, unheated/heated, non-insulated tissue with a pair of arbitrarily located vessels and general Dirichlet boundary conditions. The most important results from this study are that the effect of fluctuations on the vessel–vessel and vessel–tissue heat transfer rates can be significant. Therefore, in some situations, it will be necessary to model these fluctuations to accurately evaluate the tissue temperature distributions.

Appendix A

The purpose of this appendix is to show how $2(2N+1)$ constants (A'_{01}, A'_{02}, A'_{n1}, A'_{n2}, B'_{n1} and B'_{n2}) of Eq. (22) can be evaluated by constructing a linear system of $2(2N+1)$ equations.

$$\begin{aligned}T &= A_{01} + A'_{01}\ln(R_1^*) + A'_{02}\ln(R_2^*) \\ &+ \sum_{n=1}^{\infty} A_{n1}\{(R_1^*)^n - (R_1^*)^{-n}\}\sin(n\alpha_1) \\ &+ \sum_{n=1}^{\infty} A_{n2}\{(R_2^*)^n - (R_2^*)^{-n}\}\sin(n\alpha_2) \\ &+ \sum_{n=1}^{\infty} B_{n1}\{(R_1^*)^n - (R_1^*)^{-n}\}\cos(n\alpha_1) \\ &+ \sum_{n=1}^{\infty} B_{n2}\{(R_2^*)^n - (R_2^*)^{-n}\}\cos(n\alpha_2) \\ &+ \sum_{n=1}^{\infty} S_{A_{n1}}(R_1^*)^{-n}\sin(n\alpha_1) \\ &+ \sum_{n=1}^{\infty} S_{B_{n1}}(R_1^*)^{-n}\cos(n\alpha_1) - PR^2/4 \end{aligned} \tag{22}$$

The following relationships, mentioned in the nomenclature section, relate the variables $(R, R_1^*, \alpha_1, R_2^*, \alpha_2)$ of Eq. (22) to the original coordinates (X_1, and Y_1):

$$R^2 = X_1^2 + Y_1^2 \tag{A.1}$$

$$(R_i^*)^2 = (U_i)^2 + (V_i)^2, \quad i = 1,2 \tag{A.2}$$

$$\alpha_1 = \tan^{-1}(V_i|U_i), \quad i = 1,2 \tag{A.3}$$

$$U_i = \{(X_i - \lambda_i)(1 - \lambda_i X_i) - \lambda_i Y_i^2\} / \{(1 - (\lambda_i X_i)^2 - (\lambda_i Y_i)^2\}, \quad i = 1,2 \tag{A.4}$$

$$V_i = \{(1 - \lambda_i^2)Y_i\} / \{(1 - \lambda_i X_i)^2 - (\lambda_i Y_i)^2\}, \quad i = 1,2 \tag{A.5}$$

$$\lambda_i = \{1 + a_{1i}a_{2i} - ((1 - a_{1i}^2)(1 - a_{2i}^2))^{1/2}\}/(a_{1i} + a_{2i}), \quad i = 1,2 \tag{A.6}$$

$$a_{1i} = A_{vi} - R_{vwi}, \quad i = 1,2 \tag{A.7}$$

$$a_{2i} = A_{vi} + R_{vwi}, \quad i = 1,2 \tag{A.8}$$

$$X_2 = X_1\cos(\phi_1) + Y_1\sin(\phi_1) \tag{A.9}$$

$$Y_2 = Y_1\cos(\phi_1) + X_1\sin(\phi_1) \tag{A.10}$$

Substituting Eqs. (A.1)–(A.10) into Eq. (22), the new Eq. (22) in the original coordinates (X_1, Y_1) can be rewritten as follows:

$$\begin{aligned}T &= A_{01} + A'_{01}\ln(R_1^*(X_1,Y_1)) + A'_{02}\ln(R_2^*(X_1,Y_1)) \\ &+ \sum_{n=1}^{\infty} A_{n1}\{(R_1^*(X_1,Y_1))^n \\ &- (R_1^*(X_1,Y_1))^{-n}\}\sin(n\alpha_1(X_1,Y_1)) \\ &+ \sum_{n=1}^{\infty} A_{n2}\{(R_2^*(X_1,Y_1))^n \\ &- (R_2^*(X_1,Y_1))^{-n}\}\sin(n\alpha_2(X_1,Y_1)) \\ &+ \sum_{n=1}^{\infty} B_{n1}\{(R_1^*(X_1,Y_1))^n \\ &- (R_1^*(X_1,Y_1))^n\}\cos(n\alpha_1(X_1,Y_1)) \\ &+ \sum_{n=1}^{\infty} B_{n2}\{(R_2^*(X_1,Y_1))^n \\ &- (R_2^*(X_1,Y_1))^{-n}\}\cos(n\alpha_2(X_1,Y_1)) \\ &+ \sum_{n=1}^{\infty} S_{A_{n1}}(R_1^*(X_1,Y_1))^n\sin(n\alpha_1(X_1,Y_1)) \\ &+ \sum_{n=1}^{\infty} S_{B_{n1}}(R_1^*(X_1,Y_1))^{-n}\cos(n\alpha_1(X_1,Y_1)) \\ &- PR^2(X_1,Y_1)/4 \end{aligned} \tag{A.11}$$

The original coordinates (X_1, Y_1) relate to the vessel 1 parameters (R_{vw1}, θ_1) and vessel 2 parameters (R_{vw2}, θ_2) as given below.

For vessel 1:

$$X_1 = R_{vw1}\cos\theta_1 + A_{v1} \tag{A.12}$$

$$Y_1 = R_{vw1}\sin\theta_1 \tag{A.13}$$

For vessel 2:

$$\begin{aligned}X_1 &= (R_{vw2}\cos\theta_2 + A_{v2})\cos(\phi_1) \\ &\quad - (R_{vw2}\sin\theta_2)\sin(\phi_1)\end{aligned} \tag{A.14}$$

$$\begin{aligned}Y_1 &= (R_{vw2}\cos\theta_2 + A_{v2})\sin(\phi_1) \\ &\quad - (R_{vw2}\sin\theta_2)\cos(\phi_1)\end{aligned} \tag{A.15}$$

Substituting Eqs. (A.12)–(A.15), respectively into Eq. (A.11) and applying the original vessel wall boundary conditions to the resulting equation, gives the following two equations:

$$\begin{aligned}F_{vw1} &= 1 + P/4 + A'_{01}\ln(R_1^*(R_{vw1},\theta_1)) \\ &\quad + A'_{02}\ln(R_2^*(R_{vw1},\theta_1)) \\ &\quad + \sum_{n=1}^{\infty} A_{n1}\{(R_1^*(R_{vw1},\theta_1))^n \\ &\quad - (R_1^*(R_{vw1},\theta_1))^{-n}\}\sin(n\alpha_1(R_{vw1},\theta_1)) \\ &\quad + \sum_{n=1}^{\infty} A_{n2}\{(R_2^*(R_{vw1},\theta_1))^n \\ &\quad - (R_2^*(R_{vw1},\theta_1))^{-n}\}\sin(n\alpha_2(R_{vw1},\theta_1)) \\ &\quad + \sum_{n=1}^{\infty} B_{n1}\{(R_1^*(R_{vw1},\theta_1))^n \\ &\quad - (R_1^*(R_{vw1},\theta_1))^{-n}\}\cos(n\alpha_1(R_{vw1},\theta_1)) \\ &\quad + \sum_{n=1}^{\infty} B_{n2}\{(R_2^*(R_{vw1},\theta_1))^n \\ &\quad - (R_2^*(R_{vw1},\theta_1))^{-n}\}\cos(n\alpha_2(R_{vw1},\theta_1)) \\ &\quad - PR^2(R_{vw1},\theta_1)/4 \end{aligned} \tag{A.16}$$

$$\begin{aligned}F_{vw2} &= 1 + P/4 + A'_{01}\ln(R_1^*(R_{vw2},\theta_2)) \\ &\quad + A'_{02}\ln(R_2^*(R_{vw2},\theta_2)) + \sum_{n=1}^{\infty} A_{n1}\{(R_1^*(R_{vw2},\theta_2))^n \\ &\quad - (R_1^*(R_{vw2},\theta_2))^{-n}\}\sin(n\alpha_1(R_{vw2},\theta_2)) \\ &\quad + \sum_{n=1}^{\infty} A_{n2}\{(R_2^*(R_{vw2},\theta_2))^n \\ &\quad - (R_2^*(R_{vw2},\theta_2))^{-n}\}\sin(n\alpha_2(R_{vw2},\theta_2)) \\ &\quad + \sum_{n=1}^{\infty} B_{n1}\{(R_1^*(R_{vw2},\theta_2))^n \\ &\quad - (R_1^*(R_{vw2},\theta_2))^{-n}\}\cos(n\alpha_2(R_{vw2},\theta_2)) \\ &\quad + \sum_{n=1}^{\infty} B_{n2}\{(R_2^*(R_{vw2},\theta_2))^n \\ &\quad - (R_2^*(R_{vw2},\theta_2))^{-n}\}\cos(n\alpha_2(R_{vw2},\theta_2)) \\ &\quad - PR^2(R_{vw2},\theta_2)/4 \end{aligned} \tag{A.17}$$

It can be seen from Eqs. (A.16) to (A.17) that they are only functions of vessel 1 and vessel 2 parameters, respectively. Multiplying both sides of Eq. (A.16) with $\sin(m\theta_1)$ and $\cos(m\theta_1)$, respectively (where, $m = 0,\ldots,N$), and integrating over the vessel 1 perimeter ($\theta_1 = 0,\ldots,2\pi$) will result in a linear system of $2N+1$ equations with $2(2N+1)$ unknowns. Similarly, multiplying both sides of Eq. (A.17) with $\sin(m\theta_2)$ and $\cos(m\theta_2)$, respectively (where, $m = 0,\ldots,N$), and integrating over the vessel 2 perimeter ($\theta_2 = 0,\ldots,2\pi$) will result in an additional linear system of $2N+1$ equations with $2(2N+1)$ unknowns. This complete set of $2(2N+1)$ equations with $2(2N+1)$ unknowns can be solved using any linear equation solver to evaluate the constants.

References

[1] D.A. Pabst, S.A. Rommel, W.A. McLellan, T.M. Williams, T.K. Rowles, Thermoregulation of the intra-abdominal testes of the bottlenose Dolphin (*Tursiops truncatus*) during exercise, J. Exp. Biol. 198 (1995) 221–226.

[2] C.M. Muth, B. Mainzer, J. Peters, The use of counter-current heat exchangers diminishes accidental hypothermia during abdominal aortic aneurysm surgery, Acta Anesthesiol. Scand. 40 (1996) 1197–1202.

[3] B.I. Tieleman, J.B. Williams, G. Michaeli, B. Pinshow, The role of the nasal passages in the water economy of crested larks and desert larks, Physiol. Biochem. Zool. 72 (2) (1999) 219–226.

[4] N.R. Geist, Nasal respiratory turbinate function in birds, Physiol. Biochem. Zool. 73 (5) (2000) 581–589.

[5] C. Jessen, Selective brain cooling in mammals and birds, Jpn. J. Physiol. 51 (2001) 291–301.

[6] M.W. Dae, D.W. Gao, P.C. Ursell, C.A. Stillson, D.I. Sessler, Safety and efficacy of endovascular cooling and rewarming for induction and reversal of hypothermia in human sized pigs, Stroke 34 (2003) 734–738.

[7] S.A. Rommel, H. Caplan, Vascular adaptations for heat conservation in the tail of Florida manatees (*Trichechus manatus latirostris*), J. Anat. 202 (2003) 343–353.

[8] J.W. Mitchell, G.E. Myers, An analytical model of the counter-current heat exchange phenomena, Biophys. J. 8 (1968) 897–911.

[9] J.C. Chato, Heat transfer to blood vessels, J. Biomech. Eng. 102 (1980) 110–118.

[10] E.H. Wissler, An analytical solution countercurrent heat transfer between parallel vessels with a linear axial temperature gradient, J. Biomech. Eng. 110 (1988) 254–256.

[11] C.K. Charny, R.L. Levin, Heat transfer normal to paired arterioles and venules embedded in perfused tissue during hyperthermia, J. Biomech. Eng. 110 (1988) 277–282.

[12] Z. Chen, R.B. Roemer, The effects of large blood vessels on temperature distributions during simulated hyperthermia, J. Biomech. Eng. 114 (1992) 473–481.

[13] H. Brinck, J. Werner, Estimation of the thermal effects of blood flow in a branching counter-current network using a three dimensional vascular model, J. Biomech. Eng. 116 (1994) 324–330.

[14] G.M.J. Van Leeuwen, A.N.T.J. Kotte, J. Crezee, J.J.W. Lagendijk, Tests of the geometrical description of blood vessels in a thermal model using counter-current geometries, Phys. Med. Biol. 42 (1997) 1515–1532.

[15] A. Shitzer, L.A. Stroschein, R.R. Gonzalez, K.B. Pandolf, Numerical analysis of an extremity in cold environment including counter-current arterio-venous heat exchange, J. Biomech. Eng. 119 (1997) 179–186.

[16] S. Weinbaum, L.X. Xu, L. Zhu, A. Ekpene, A new fundamental bioheat equation for muscle tissue: Part 1—Blood perfusion term, J. Biomech. Eng. 119 (1997) 278–288.

[17] W. Roetzl, Y. Xuan, Transient response of the human limb to an external stimulus, Int. J. Heat Mass Transfer 41 (1) (1998) 229–239.
[18] J. Song, L.X. Xu, D.E. Lemons, S. Weinbaum, Microvascular thermal equilibration in rat spinotrapezius muscle, Ann. Biomed. Eng. 27 (1997) 56–66.
[19] L. Zhu, Theoretical evaluation of contributions of heat conduction and counter-current heat exchange in selective brain cooling in humans, Ann. Biomed. Eng. 28 (2000) 269–277.
[20] C. Chen, L.X. Xu, A vascular model for heat transfer in an isolated pig kidney during water bath heating, J. Heat Transfer 125 (2003) 936–943.
[21] M.M. Chen, K.R. Holmes, Microvascular contributions in tissue heat transfer, Ann. NY Acad. Sci. 335 (1980) 137–150.
[22] R.F. Di Felice Jr., H.H. Bau, Conductive heat transfer between eccentric cylinders with boundary conditions of the third kind, J. Heat Transfer 105 (1983) 678–680.
[23] S. Weinbaum, L.M. Jiji, A new simplified bioheat equation for the effect of blood flow on local average tissue temperature, J. Biomech. Eng. 107 (1985) 131–139.
[24] J.W. Baish, P.S. Ayyaswamy, Small-scale temperature fluctuations in perfused tissue during local hyperthermia, J. Biomech. Eng. 108 (1986) 246–250.
[25] M. Zhu, S. Weinbaum, L.M. Jiji, D.E. Lemons, On the generalization of the Weinbaum–Jiji bioheat equation to microvessels of unequal size; the relation between the near field and local average tissue temperatures, J. Biomech. Eng. 110 (1988) 74–81.
[26] M. Zhu, S. Weinbaum, L.M. Jiji, Heat exchange between unequal countercurrent vessels asymmetrically embedded in a cylinder with surface convection, Int. J. Heat Mass Transfer 33 (10) (1990) 2275–2283.
[27] Y.L. Wu, S. Weinbaum, L.M. Jiji, A new analytic technique for 3-D heat transfer from a cylinder with two or more axially interacting eccentrically embedded vessels with application to countercurrent blood flow, Int. J. Heat Mass Transfer 36 (4) (1993) 1073–1083.
[28] L. Zhu, D.E. Lemons, S. Weinbaum, A new approach for predicting the enhancement in the effective conductivity of perfused muscle tissue due to hyperthermia, Ann. Biomed. Eng. 23 (1995) 1–12.
[29] L. Zhu, D.E. Lemons, S. Weinbaum, Microvascular thermal equilibration in rat cremaster muscle, Ann. Biomed. Eng. 24 (1996) 109–123.
[30] D. Shrivastava, B. McKay, R.B. Roemer, An analytical study of heat transfer in finite tissues with two blood vessels and uniform Dirichlet boundary conditions, J. Heat Transfer 127 (2005) 179–188.
[31] R.B. Roemer, A.W. Dutton, A generic tissue convective energy balance equation: Part 1. Theory and derivation, J. Biomech. Eng. 120 (1998) 395–404.
[32] D. Shrivastava, R.B. Roemer, An analytical derivation of source term dependent, 2-D generalized Poisson conduction shape factors, Int. J. Heat Mass Transfer 47 (19–20) (2004) 4293–4300.
[33] L.X. Xu, K.R. Holmes, B. Moore, M.M. Chen, H. Arkin, Microvascular architecture with in the pig kidney cortex, Microvasc. Res. 47 (1994) 293–307.
[34] S.G. Klemick, M.A. Jog, P.S. Ayyaswamy, Numerical evaluation of heat clearance properties of a radiatively heated biological tissue by adaptive grid scheme, Numer. Heat Transfer Part A 31 (1997) 451–467.
[35] H.H. Pennes, Analysis of tissue and arterial blood temperatures in resting human forearm, J. Appl. Physiol. 1 (1948) 93–122.
[36] J.W. Brown, R.V. Churchill, Complex Variables and Applications, McGraw-Hill, Inc., NewYork, 1996.
[37] G.E. Myers, Analytical Methods in Conduction Heat Transfer, AMCHT Publications, Madison, WI, 1998.
[38] Devashish, Development of an improved thermal model to predict in-vivo tissue temperatures, Ph.D. Dissertation, University of Utah, Salt Lake City, UT, 2004.
[39] M.A. Mackey, W.C. Dewey, Time-temperature analyses of cell killing of synchronous G1 and S phase Chinese hamster cells in vitro, Radiat. Res. 113 (1988) 318–333.
[40] A.N. Guthkelch, L.P. Carter, J.R. Cassady, K.H. Hynynen, R.P. Iacono, P.C. Johnson, E.A.M.T. Obbens, R.B. Roemer, J.F. Seeger, D.S. Shimm, B. Stea, Treatment of malignant brain tumors with focused ultrasound hyperthermia and radiation: results of a phase 1 trial, J. Neuro-Oncol. 10 (1991) 271–284.
[41] H. Wehner, A.V. Ardenne, S. Kaltofen, Whole-body hyperthermia with water-filtered infrared radiation: technical-physical aspects and clinical experiences, Int. J. Hyperthermia 17 (1) (2001) 19–30.
[42] M.C. Kolios, M.D. Sherar, J.W. Hunt, Large blood vessel cooling in heated tissues: a numerical study, Phys. Med. Biol. 40 (1995) 477–494.
[43] J. Song, L.X. Xu, D.E. Lemons, S. Weinbaum, Enhancement in the effective thermal conductivity in rat spinotrapezius due to vasoregulation, J. Biomech. Eng. 119 (1997) 461–468.
[44] W.R. Milnor, Cardiovascular Physiology, Oxford University Press, New York, 1990.
[45] H. Gray, Gray's anatomy, descriptive and surgical, Running Pr, 1978.